Magnetic Resonance in Medicine 63:1703–1707 (2010)

# Comparative SNR for High-Throughput Mouse Embryo MR Microscopy

Xiaoli Zhang,[1,2]* Jurgen E. Schneider,[3] Sharon Portnoy,[1] Shoumo Bhattacharya,[3] and R. Mark Henkelman[1,2]

**MR microscopy is being explored as a useful imaging tool to phenotype mouse embryos due to its volume coverage with three-dimensional isotropic resolution. However, the main limitation for mouse embryo MR microscopy is the signal-to-noise ratio. Large numbers of embryos are needed for phenotypic screening, making high throughput essential. Two high-throughput imaging approaches, multi-embryo shared-coil (shared) and multi-embryo individual-coil (individual), have been developed for phenotyping mouse embryos. This study quantitatively compares the signal-to-noise ratio at equivalent times between these two established methods by compensating for differences that result from field strength. While the individual method provides 3.3 times as much signal-to-noise ratio as the shared method at equivalent conditions, it is more difficult and expensive to implement. Furthermore, the number of embryos that can be imaged concurrently is limited by the number of receiver channels. The objective of this study is to provide measured comparative data to guide choices for high-throughput mouse embryo MR microscopy and other similar applications. Magn Reson Med 63:1703–1707, 2010. © 2010 Wiley-Liss, Inc.**

**Key words: SNR; high throughput; MR microscopy; mouse embryo; Multiple mouse MRI**

The increased use of the mouse as a model for mammalian genetics has kindled an interest in developing strategies for distinguishing wild-type and mutant mouse embryonic anatomy and development (1–3). The potential of magnetic resonance microscopy for morphologic phenotyping of the mouse embryo has previously been demonstrated (4–8); however, high-quality images require very long scan times.

In screening studies, the number of embryos to be imaged is very large (thousands). This, in turn, requires high throughput for efficient phenotyping of embryos. Also, due to the small size of the mouse embryo, spatial resolution as fine as possible (tens of microns) is needed to resolve the detailed structure within the embryo. It is the signal-to-noise ratio (SNR) that is the major controlling limitation for achieving high-spatial-resolution images in a reasonable scan time (typically overnight scans). Thus, to achieve realistic throughput, simultaneous imaging of multiple embryos is essential.

High-throughput mouse embryo MR microscopy can been realized by two methods, as illustrated in Fig. 1: multiple embryos in a shared coil (7,8) and multiple embryos each in an individual coil that is similar to multiple mouse MRI for adult mouse imaging (9).

The objective of this study is to compare the SNR for these two established high-throughput mouse embryo MR microscopy methods: the multi-embryo shared-coil method developed at Oxford (hereafter referred as "shared") and the multi-embryo individual-coil method developed at Toronto (hereafter referred as "individual"). Although these methods have been implemented at different field strengths and scan times, these differences can be compensated to give a comparison based only on the methods of parallelization and the coils. We chose to perform this comparison between two established techniques to provide measured comparative data to guide choices for high-throughput mouse embryo MRM and other similar applications.

## MATERIALS AND METHODS

### Embryo Preparation

C57BL/6 embryos at age E15.5 days were first dissected from the dam and placed in 37°C Hanks' balanced salt solution (BSS) containing 5-mM ethylenediaminetetraacetic acid (EDTA). The embryos were then washed twice with phosphate-buffered saline, followed by immersion in 4% paraformaldehyde prepared with 1× phosphate-buffered saline and 4 μL/1 mL Gadolinium diethylenetriamine penta-acetic acid (Gd-DTPA) (Magnevist; Bayer Schering Pharma, Berlin, Germany).

One percent agarose (Seakem LE Agarose; Lonza Group Ltd, Muenchensteinerstrasse, Basel, Switzerland) was dissolved in double-distilled water and kept molten at ~65°C using a hot plate. Gd-DTPA at 4 μL/1 mL was then added to the molten agarose. A 28mm-diameter NMR tube was placed on ice, and then 22 mL of agarose was pipetted into the NMR tube and cooled. Four embryos were placed in one layer, covered with agarose, and allowed to set. Seven repeated layers were added, and then the rest of the tube was filled with agarose and allowed to set. Finally, the tube was sealed with Parafilm. This resulted in a tube containing eight layers of embryos, each mounted in gel, as seen in Fig. 1.

### High-Throughput Embryo MR Imaging

In the shared method, the 32 mouse embryos were imaged in Oxford, UK, on a 9.4-T horizontal magnet

[1]Mouse Imaging Centre, Hospital for Sick Children, Toronto, Ontario, Canada.
[2]Department of Medical Biophysics, University of Toronto, Toronto, Ontario, Canada.
[3]Department of Cardiovascular Medicine, University of Oxford, Oxford, United Kingdom.
*Correspondence to: Xiaoli Zhang, M.Sc., Mouse Imaging Centre, Hospital for Sick Children, 25 Orde Street, Toronto, Ontario, Canada M5T 3H7. E-mail: xzhang@phenogenomics.ca

Received 2 June 2009; revised 11 November 2009; accepted 16 December 2009.
DOI 10.1002/mrm.22352
Published online in Wiley InterScience (www.interscience.wiley.com).

© 2010 Wiley-Liss, Inc.

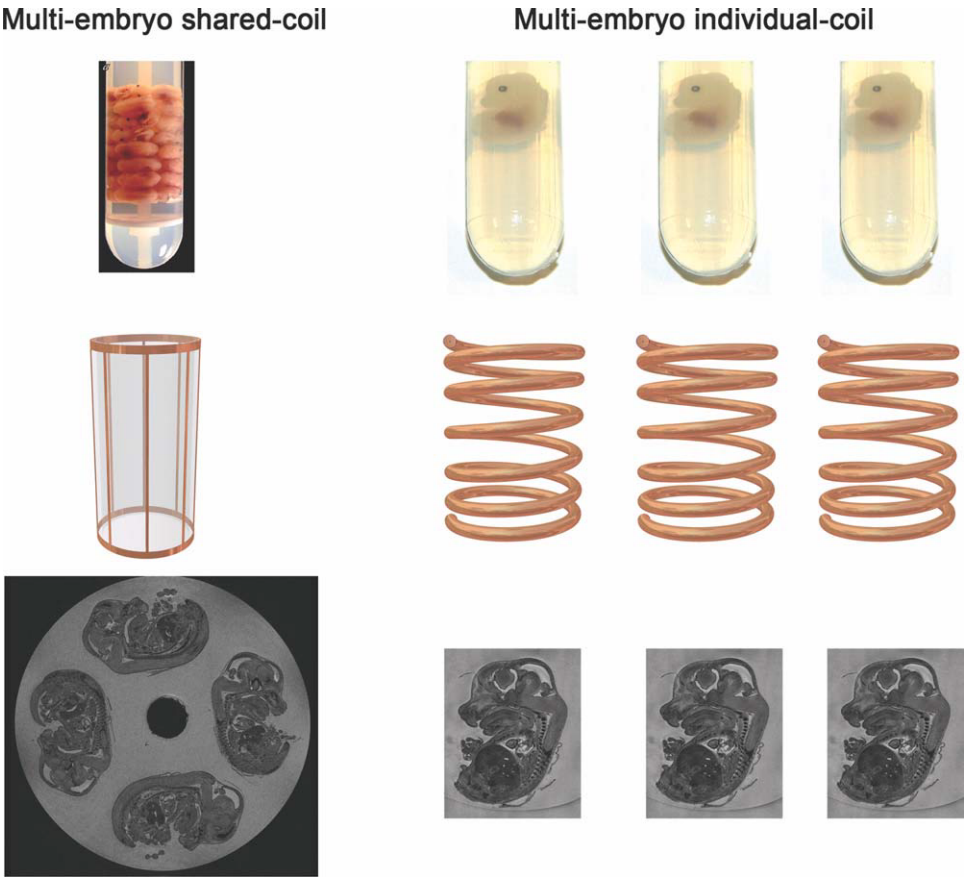


FIG. 1. Two high-throughput mouse embryo MR microscopy methods: multi-embryo shared-coil and multi-embryo individual-coil. **a:** Stack of 32 embryos embedded in a NMR tube. **b:** Schematic representation of the birdcage coil for the multi-embryo shared-coil method. **c:** A cross-sectional image of four embryos in one layer. **d:** Embryos each embedded in a small NMR tube. **e:** Schematic representation of the solenoid coils for the multi-embryo individual-coil methods. **f:** Embryonic images for the multi-embryo individual-coil method.

interfaced to a Varian VNMRS DirectDrive console (Varian Inc., Palo Alto, CA) using a quadrature radiofrequency (RF) birdcage coil with an inner diameter of 28mm and length of 56mm (Rapid Biomedical, Wurzburg, Germany) for both transmission and reception. A three-dimensional spoiled gradient echo sequence (pulse repetition time/echo time = 30/10 ms, with a 60° excitation pulse of rectangular shape) was used to obtain strong $T_1$ contrast. A matrix size of 608 × 608 × 1408 on a field of view (FOV) of 26 × 26 × 50mm$^3$ yielded a resolution of 43 × 43 × 36 μm$^3$.

For the individual method, the identical embryos were then melted out and resuspended in the same agarose solution in small NMR tubes (outer diameter: 13mm; length: 41mm) to perform the individual method image acquisition. The experiment was conducted at the Mouse Imaging Centre in Toronto, Canada, on a 7-T horizontal Varian VNMRS DirectDrive system using a custom-built array of overwound solenoid coils (inner diameter: 13.2mm; length: 18mm) (10) to image multiple embryos simultaneously with an identical pulse sequence. The matrix size was 328 × 390 × 580 on a FOV of 14 × 14 × 25mm$^3$, resulting in the same spatial resolution as the shared method of 43 × 36 × 43 μm$^3$. Details of the imaging parameters for both experiments are listed in Table 1.

Reconstruction of both MR images was performed in an identical manner, without using zero-filling or applying low-pass filters to the raw data.

## Relaxation Time Measurements

To compensate for the effect on SNR caused by the relaxation time differences at the two field strengths, $T_1$ and $T_2$* for the mouse embryo were measured at both laboratories. In Oxford, $T_1$ measurements were performed by using an inversion-recovery two-dimensional gradient echo sequence; 16 inversion times were exponentially arrayed between 10 ms and 2000 ms (pulse repetition time/echo time = 2100/1.8 ms, matrix size 128 × 128, FOV = 30 × 30mm$^2$, eight slices, slice thickness 0.5mm, gap 0.4mm). In Toronto, an identical pulse sequence was used for $T_1$ measurement, except echo time = 6.5 ms and FOV = 20 × 20mm$^2$. In both Oxford and Toronto, $T_2$* measurements were achieved using a two-dimensional gradient echo sequence with pulse repetition time = 61.8 ms, and echo times varied in 18 values (echo time

Table 1
Imaging Protocols for the Two High-Throughput Mouse Embryo MR Microscopy Methods

| | Field ($B_0$) | RF coil | FOV (mm$^3$) | Matrix size | Resolution (μm$^3$) | NEX | T (hours) |
|---|---|---|---|---|---|---|---|
| Shared | 9.4 T | Quadrature birdcage | 26 × 26 × 50 | 608 × 608 × 1408 | 43 × 43 × 36 | 4 | 12.3 |
| Individual | 7 T | Solenoid | 14 × 14 × 25 | 328 × 390 × 580 | 43 × 36 × 43 | 4 | 4.3 |

Table 2
Quality Factor (Q) Measurements

| | Unloaded Q | Loaded Q | $R_S/R_C$ |
|---|---|---|---|
| Shared | 303 | 178 | 0.70 ± 0.05 |
| Individual | 139 | 68 | 1.06 ± 0.19 |

= 3.2, 4, 5, 6, 7, 8, 9, 10, 12, 15, 20, 25, 30, 35, 40, 45, 50, 55 ms). The matrix size was 100 × 178, FOV = 14 × 25mm$^2$, one slice of thickness 0.5mm for the single tube scan, and 16 slices (slice thickness 0.5mm, slice gap 1mm) and a FOV of 30 × 30mm$^2$, matrix size 256 × 256 for the multi-embryo scan, respectively. Both $T_1$ and $T_2$* were measured on each of three tissues: brain, heart, and liver.

### Quality Factor (Q) Measurements

The experimental quality factors (Q) of the birdcage and solenoid coils were measured for the unloaded coil ($Q_U$), as well as for the coil loaded with mouse embryo(s) ($Q_L$), using a network analyzer (Agilent 4395A, Palo Alto, CA). The Q values were determined as the resonant frequency divided by the 3-dB bandwidth in the reflection response curve (11). The ratio between sample resistance ($R_{sample}$) and coil resistance ($R_{coil}$) was determined by $R_{sample}/R_{coil} = Q_U/Q_L - 1$.

### Image Processing

To ensure the accuracy of the SNR comparison, identical volumes of interest were chosen on three embryo images from both the shared and individual methods. This was achieved by computer segmenting the embryo from the surrounding agarose gel in the image, using segmentation software ITK-SNAP (12), followed by intensity-based nonlinear image registration using a customized code to register the six images. Three spherically shaped volumes of interest in the brain, heart, and liver were then defined equivalently in each of the registered embryonic images to calculate signal intensity. Each volume of interest had a margin of at least two pixels from the tissue boundary in all slices. The MR noise was defined as the standard deviation of the magnitude image in an artifact-free background region.

### SNR Compensation

The MR signal for a spoiled gradient echo sequence is given by (13)

$$S = M_0 \times \sin\theta \times \frac{1 - e^{-TR/T1}}{1 - e^{-TR/T1}\cos\theta} \times e^{-TE/T2^*} \qquad [1]$$

where $M_0$ is the magnetization, and θ is the flip angle. Therefore, the SNR of the individual method was multiplied by the factor

$$\varepsilon = \frac{1 - e^{-TR/T1_I}\cos\theta}{(1 - e^{-TR/T1_I})e^{-TE/T2_I^*}} \times \frac{(1 - e^{-TR/T1_S})e^{-TE/T2_S^*}}{1 - e^{-TR/T1_S}\cos\theta} \qquad [2]$$

to compensate for the SNR difference caused by different relaxation times. The subscripts "S" and "I" refer to the shared and individual methods, respectively.

MR signal is proportional to $B_0^2$, and MR noise due to the sample and the coil losses is

$$\sqrt{4k\Delta f\left(R_{sample}T_{sample} + R_{coil}T_{coil}\right)} = \sqrt{4k\Delta f R_{sample}T_{sample}\left(1 + Q_L T_{coil}/\left((Q_U - Q_L)T_{sample}\right)\right)},$$

where $T_{sample}$ and $T_{coil}$ are temperature of the sample and coil, k is the Boltzmann constant, and $\Delta f$ is the receiver bandwidth. The sample resistance of a cylindrical sample is $R_{sample} = \pi\omega_0^2 B_1^2 l r^4/(8\rho)$, where $\omega_0 = \gamma B_0$ is the Larmor frequency, $B_1$ is the magnetic field induced in the RF coil per unit current, l is the length of the cylindrical sample, $r$ is the radius of the cylindrical sample, and $\rho$ is the resistivity of the sample (14). It can be seen that the sample resistance $R_{sample}$ is proportional to the square of field strength. The multiplicative factor

$$\alpha = \sqrt{\frac{1 + Q_{L,I}T_{Coil}/\left[(Q_{U,I} - Q_{L,I})T_{Sample}\right]}{1 + Q_{L,S}T_{Coil}/\left[(Q_{U,S} - Q_{L,S})T_{Sample}\right]}} \times \frac{B_{0,S}}{B_{0,I}} \qquad [3]$$

was therefore used to correct for coil and sensitivity of the SNR measured at 7 T to a new field strength of 9.4 T. The temperatures of the coil ($T_{coil}$) and sample ($T_{sample}$) were taken to be 290 K. The term $B_{0,S}/B_{0,I}$ corrects for the fact that the intrinsic SNR scales with field strength where the "I" and "S" in subscripts stand for the individual and shared methods.

Since the SNR for MRI increases as the square root of the acquisition time, a factor $(T_S/T_I)^{1/2}$ was used to compensate for SNR of the individual method due to the differences in acquisition time.

## RESULTS

The measured quality factors for the two experimental setups are listed in Table 2. The sample resistance to coil resistance ratio was determined from the unloaded and loaded Qs to be 0.70 ± 0.05 and 1.06 ± 0.19 for the shared and individual methods, respectively.

Representative mouse embryo MR images from the shared and individual methods are shown in Fig. 2 for the same embryo after segmenting embryos from gel and image registration to give views at equivalent sections. It can be seen that both the original MR images have sufficiently high quality to resolve fine structures such as the heart chambers. Measured SNRs from both methods and the SNRs compensated for different experimental conditions are listed in Table 3. The measured SNRs for the different tissues are quite variable. However, the SNR ratios at equivalent experimental conditions after compensating for scan time, field strength, and relaxation times are consistent over the different tissues. The SNR of the multi-embryo individual-coil approach is 3.3 times the SNR of the multi-embryo shared-coil at equivalent conditions.

## DISCUSSION AND CONCLUSION

Both the multi-embryo shared-coil and the multi-embryo individual-coil high-throughput mouse embryo MR microscopy methods provide image quality that allows for visual analysis and automated computer processing

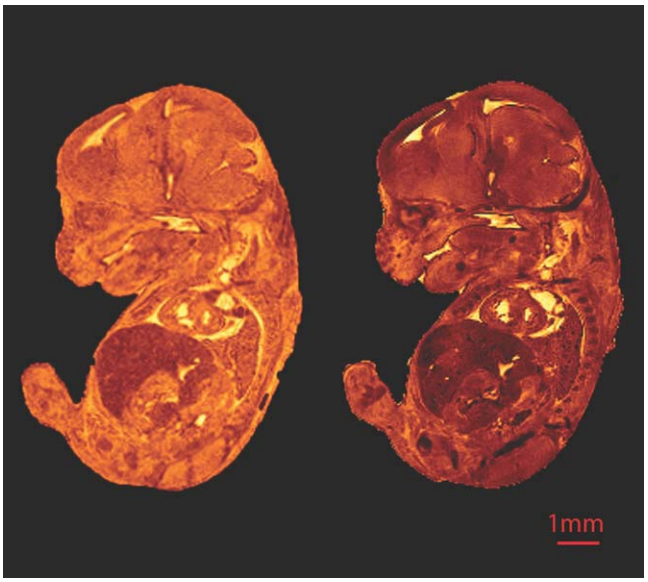


FIG. 2. Segmented and registered images from the same embryo: shared method (left); individual method (right).

(15,16). The individual coil method is more complex in terms of the need for multiple receivers and it requires a higher cost to implement. In addition, the number of embryos that can be imaged simultaneously for the individual method is limited by the number of receiver channels (in this case, 16). While the shared coil method is easy to implement and is more modest in cost, it poses some challenges on the reconstruction side due to the seven-times-larger data set (~4 GB of raw data). After compensating for the differences in the experimental conditions such as field strength, relaxation time, and acquisition time, the individual coil method provides about 3.3 times higher SNR at equivalent experimental conditions. Much of the contribution to the 3.3 times higher SNR can be understood in terms of the "volume filling factor" (17). The ratio of the coil geometric volumes (18) between small solenoid coil and large birdcage coil is $(\pi \times 13.2^2 \times 18/4)/(\pi \times 28^2 \times 56/4) = 1/14$, which would lead to simplistic estimation of the ratio of the SNRs to be $(1/14)^{-1/2} \approx 3.74$. However, this estimation does not account for coil type (birdcage versus solenoid), noise sources (sample versus coil), $B_1$ distribution, or increased noise from multiple embryos. Thus, direct experimental measurements were needed.

In terms of overall throughput, 32 and 16 embryos can be imaged concurrently for the shared and individual methods, respectively. Since the SNR of MR images is proportional to the square root of scan time, the throughput of the individual method is $3.3^2 \times 16/32 = 5.4$ times that of the shared method at the same experimental conditions (field strength, resolution, SNR).

The MR noise is contributed by both sample noise and coil noise, which have different dependencies on field strength and coil dimensions. The sample noise is caused primarily by currents induced in the tissue by the electric and magnetic fields of the RF coil. Generally, little can be done to reduce currents generated by the magnetic field. However, the coil noise can be reduced

Table 3
$T_1$, $T_2^*$, SNR Measurements, and SNR Compensation for the Two Methods

| | Shared method | | | Individual method | | | SNR compensation | | | | |
|---|---|---|---|---|---|---|---|---|---|---|---|
| | $SNR_{meas}$ | $T_1$ (ms) | $T_2^*$ (ms) | $SNR_{meas}$ | $T_1$ (ms) | $T_2^*$ (ms) | Scan time | $T_1$, $T_2^*$ ($\varepsilon$) | $B_0$ | $SNR_{corr}$ | SNR ratio |
| Brain | 9.7 ± 0.2 | 148 ± 6 | 13.9 ± 0.1 | 18.4 ± 1.7 | 134 ± 3 | 16.8 ± 0.5 | 1.699 | 0.82 ± 0.003 | 1.2 ± 0.2 | 30.63 ± 2.4 | 3.16 ± 0.31 |
| Heart | 6.7 ± 0.2 | 162 ± 7 | 9.3 ± 0.2 | 12.8 ± 1.4 | 160 ± 6 | 10.3 ± 0.3 | | 0.89 ± 0.004 | | 23.12 ± 1.7 | 3.45 ± 0.34 |
| Liver | 11.4 ± 0.1 | 111 ± 5 | 6.4 ± 0.1 | 23.2 ± 0.8 | 94 ± 2 | 9.7 ± 0.3 | | 0.53 ± 0.003 | | 24.74 ± 2.7 | 3.20 ± 0.25 |
| Average SNR ratio | | | | | | | | | | | 3.27 ± 0.30 |

by constructing RF coils with superconducting materials to significantly lower coil resistance or by cooling the conventional coil to low temperature with liquid nitrogen or liquid helium (19,20).

When imaging even earlier-stage embryos than we have considered here (i.e., E9.5-E13.5), the sample noise decreases more rapidly than the coil noise with respect to dimensional size: the sample noise variance scales with dimension to the fifth power, whereas the coil noise variance scales with the square of dimension (14). This will result in MR image noise dominated by coil noise. In this scenario, reducing coil noise by cooling the RF coil would be beneficial for SNR (19). However, this is particularly challenging for the individual method since the space for each RF coil is very limited.

If one were to perform mouse embryo imaging at higher field strength (which would be recommended to increase the SNR), since the sample resistance is proportional to the square of field strength, whereas the coil resistance is proportional to the square root of field strength (14), MR image noise will return to the sample-noise-dominated regimen, as is the case for clinical MRI at 1.5-3 T. This will result in the SNR being proportional to the field strength for both the shared and individual methods. Therefore, at a given field strength, the SNR ratio between these two methods will no longer be dependent on the field strength and will be higher than the SNR ratio at lower field strength, as determined in this work.

This paper has conducted the first direct SNR comparison between two high-throughput mouse embryo MR microscopy methods. The individual method provides 3.3 times the SNR of the shared method at equivalent conditions after compensating for differences in field strength, scan time, and relaxation times. The advantages and disadvantages of both methods are compared to provide a general guideline for mouse embryo MR microscopy, as well other similar MR microscopy applications.

## ACKNOWLEDGMENTS

This project was funded by Genome Canada through the Ontario Genomics Institute (2008-OGI-TD-03) and the British Heart Foundation (J.E.S. and S.B.). R.M.H. holds a Canada Research Chair in Imaging. We thank Mojdeh Zamyadi and Leila Baghadi for their assistance with the image registration and segmentation and Ms. Angela Franklin and Ms. Hannah Barnes for help with the sample preparation.

## REFERENCES

1. Collins FS, Rossant J, Wurst W. A mouse for all reasons. Cell 2007; 128:9–13.
2. Hrabe de Angelis MH, Flaswinkel H, Fuchs H, Rathkolb B, Soewarto D, Marschall S, Heffner S, Pargent W, Wuensch K, Jung M, Reis A, Richter T, Alessandrini F, Jakob T, Fuchs E, Kolb H, Kremmer E, Schaeble K, Rollinski B, Roscher A, Peters C, Meitinger T, Strom T, Steckler T, Holsboer F, Klopstock T, Gekeler F, Schindewolf C, Jung T, Avraham K, Behrendt H, Ring J, Zimmer A, Schughart K, Pfeffer K, Wolf E, Balling R. Genome-wide, large-scale production of mutant mice by ENU mutagenesis. Nat Genet 2000;25:444–447.
3. Nolan PM, Peters J, Strivens M, Rogers D, Hagan J, Spurr N, Gray IC, Vizor L, Brooker D, Whitehill E, Washbourne R, Hough T, Greenaway S, Hewitt M, Liu X, McCormack S, Pickford K, Selley R, Wells C, Tymowska-Lalanne Z, Roby P, Glenister P, Thornton C, Thaung C, Stevenson JA, Arkell R, Mburu P, Hardisty R, Kiernan A, Erven A, Steel KP, Voegeling S, Guenet JL, Nickols C, Sadri R, Nasse M, Isaacs A, Davies K, Browne M, Fisher EM, Martin J, Rastan S, Brown SD, Hunter J. A systematic, genome-wide, phenotype-driven mutagenesis programme for gene function studies in the mouse. Nat Genet 2000; 25:440–443.
4. Smith BR, Johnson GA, Groman EV, Linney E. Magnetic resonance microscopy of mouse embryos. Proc Natl Acad Sci U|S|A 1994;91: 3530–3533.
5. Smith BR, Linney E, Huff DS, Johnson GA. Magnetic resonance microscopy of embryos. Comput Med Imaging Graph 1996;20:483–490.
6. Petiet AE, Kaufman MH, Goddeeris MM, Brandenburg J, Elmore SA, Johnson GA. High-resolution magnetic resonance histology of the embryonic and neonatal mouse: a 4D atlas and morphologic database. Proc Natl Acad Sci U|S|A 2008;105:12331–12336.
7. Pieles G, Geyer SH, Szumska D, Schneider J, Neubauer S, Clarke K, Dorfmeister K, Franklyn A, Brown SD, Bhattacharya S, Weninger WJ. microMRI-HREM pipeline for high-throughput, high-resolution phenotyping of murine embryos. J Anat 2007;211:132–137.
8. Schneider JE, Bose J, Bamforth SD, Gruber AD, Broadbent C, Clarke K, Neubauer S, Lengeling A, Bhattacharya S. Identification of cardiac malformations in mice lacking Ptdsr using a novel high-throughput magnetic resonance imaging technique. BMC Dev Biol 2004;4:16.
9. Bock NA, Konyer NB, Henkelman RM. Multiple-mouse MRI. Magn Reson Med 2003;49:158–167.
10. Idziak S, Haeberlen U. Design and construction of a high homogeneity RF coil for solid-state multiple-pulse NMR. J Magn Reson 1982; 50:281–288.
11. Odoj F, Rommel E, Kienlin MV, Haase A. A superconducting probehead applicable for nuclear magnetic resonance microscopy at 7 T. Rev Sci Instr 1998;69:2708–2712.
12. Yushkevich PA, Piven J, Hazlett HC, Smith RG, Ho S, Gee JC, Gerig G. User-guided 3D active contour segmentation of anatomical structures: significantly improved efficiency and reliability. Neuroimage 2006;31:1116–1128.
13. Bernstein MA, King KF, Zhou XJ. Handbook of MRI pulse sequences. msterdam: Academic Press; 2004. 1040 p.
14. Hoult DI, Lauterbur PC. The sensitivity of the zeugmatographic experiment involving human samples. J Magn Reson 1979;34: 425–433.
15. Zamyadi M, Henkelman RM, Bhattacharya S, Schneider JE, Sled JG. Registration of 3D MR images of the mouse embryos. In: Proceedings of the ISMRM 16th Annual Meeting, Toronto, 2008. p 3099.
16. Baghdadi L, Sled JG, Schneider JE, Henkelman RM, Lerch JP. Semiautomatic segmentation of mouse embryo MRIs. In: Proceedings of the ISMRM 17th Annual Meeting, Honolulu, 2009. p 2886.
17. Abragam A. The principles of nuclear magnetism. Oxford: Clarendon Press; 1961.599 p.
18. Hoult DI, Richards RE. The signal-to-noise ratio of the nuclear magnetic resonance experiment. J Magn Reson 1976;24:77–85.
19. Ratering D, Baltes C, Nordmeyer-Massner J, Marek D, Rudin M. Performance of a 200-MHz cryogenic RF probe designed for MRI and MRS of the murine brain. Magn Reson Med 2008;59:1440–1447.
20. Nouls JC, Izenson MG, Greeley HP, Johnson GA. Design of a superconducting volume coil for magnetic resonance microscopy of the mouse brain. J Magn Reson 2008;191:231–238.